GFD 2013 Lecture 10: Gravity currents on slopes and in turbulent environments

Paul Linden; notes by Gregory Wagner and Barbara Zemskova

June 28, 2013

1   Introduction

Natural gravity currents are often found flowing down slopes. Examples include the flow of hot ash down the flank of a volcano, to snow avalanches down the sides of mountains, to the flow of dense water from saline seas or silty rivers into the ocean and down a continental slope. The tilting of a gravity current down a slope adds new physics to the problem, in particular the process of entrainment of ambient fluid into the current can be important (which in flows on flat surfaces in largely suppressed by density stratification).

2   Gravity currents on slopes

2.1   Finite volume current

A finite volume gravity current can be studied with an experimental apparatus involving the sudden release of a fixed volume of dense fluid into a lighter fluid. A diagram of an experimental apparatus is shown in Figure 1. Images from a finite volume release experiment on six different slopes is shown in Figure 2, and streak photos showing the fluid motion within the current for an experiment on a $20°$ slope are shown in Figure 3.

The relevant parameters in a finite volume release and their dimensions are

g'	reduced gravity (without taking slope angle into account)	$[L/T^2]$;
Q_0	current volume / width	$[L^2]$;
θ	slope angle	no units.

The only combinations of parameters which give the correct units for velocity, length, and height of the current are then

$$U = \left(g'\right)^{1/2} Q_0^{1/4} f_0(\theta),$$
$$\{L, h\} = Q_0^{1/2} f_{1,2}(\theta). \tag{1}$$

We also expect the entrainment, which we characterize by a "rate of entrainment" velocity u_e to scale with the velocity of the flow such that

$$u_e \sim U, \tag{2}$$

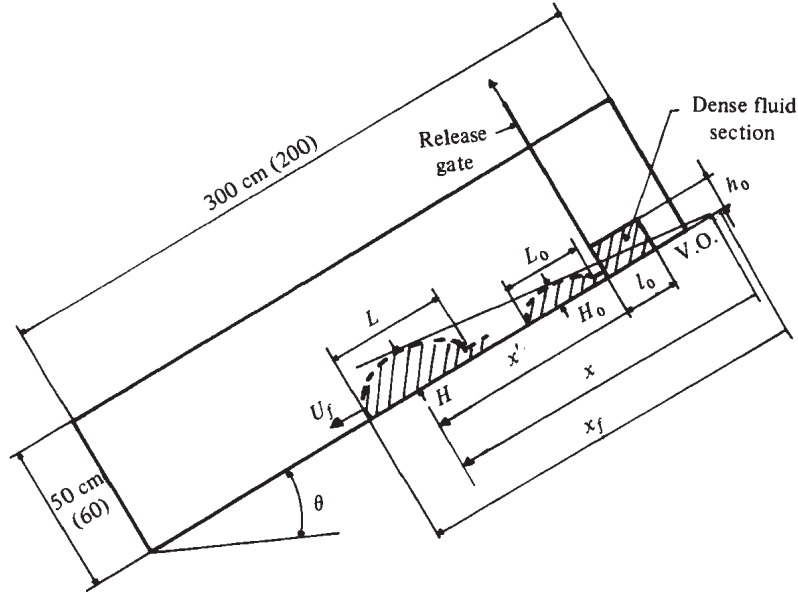where in the regime we are interested in, U is constant. We can then conclude that

Figure 1: Diagram of experimental apparatus for finite volume release of dense fluid on a slope [1].

1. the volume of the current increases linearly in time, and therefore

2. both L and h increase linearly in time because the shape of current is self-similar.

One particularly interesting point is that due to the flow structure within the current, most of the fluid entrained from the ambient environment enters at the rear of the flow. This is particularly apparent in the low Reynolds number limit for the 90° angle current, where the falling dense fluid is simply a negatively buoyant vortex ring. The scaling of the height and length of the current with time are plotted in Figure 4, and the increase in the height of the current as a function of the slope angle (which we denoted $f_2(\theta)$) is plotted in Figure 5. A plot of the dimensionless front velocity is shown as a function of distance in Figure 6 – note that the range of velocities is small even for a large range of slope angles.
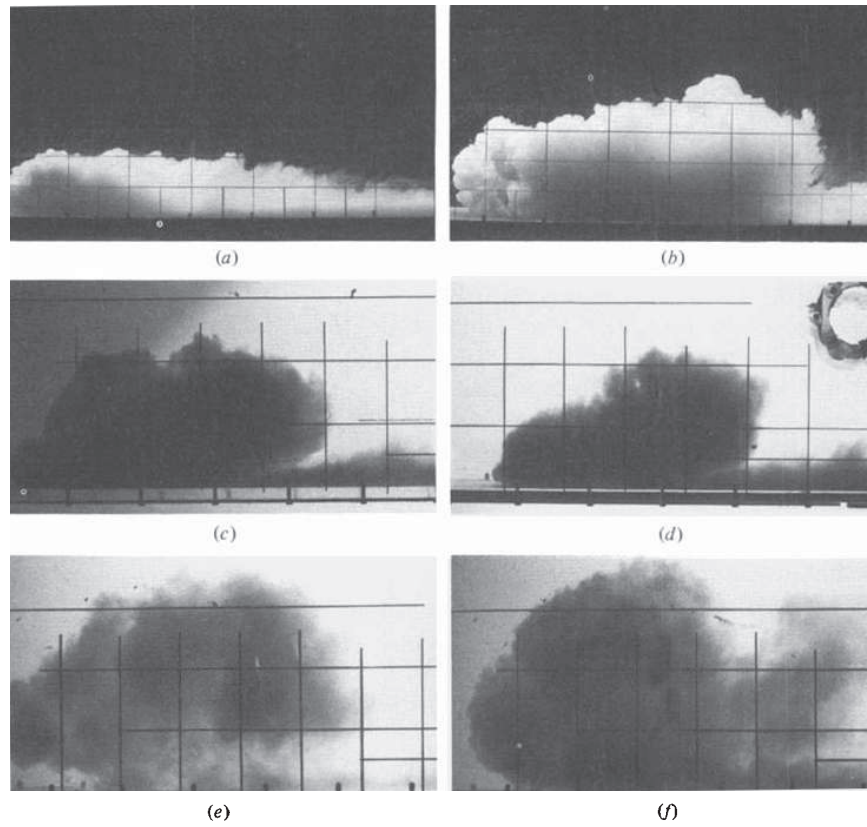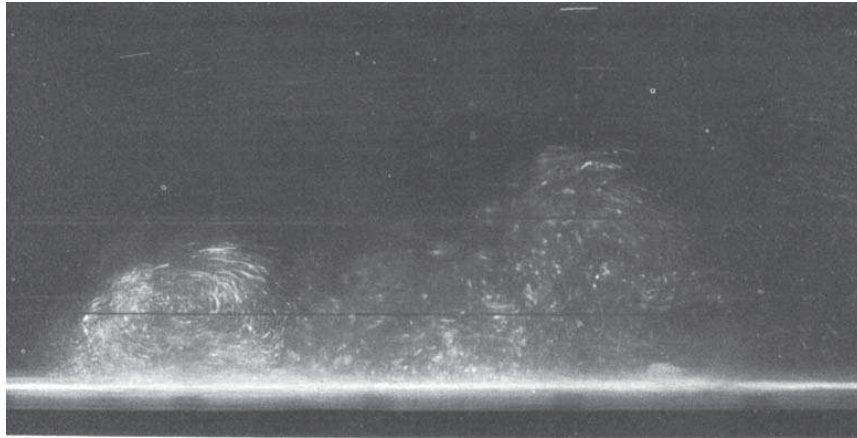
Figure 2: Finite volume release of dense fluid on a slopes angled at 5, 15, 45, 60, and 90°
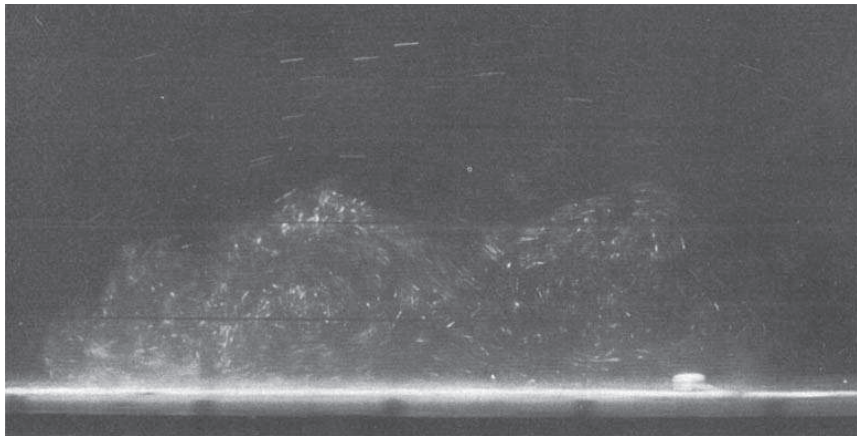(images a–f respectively). [1].

(a)

Figure 3: Streak photos of finite volume release of dense fluid on a 20° slope [1].
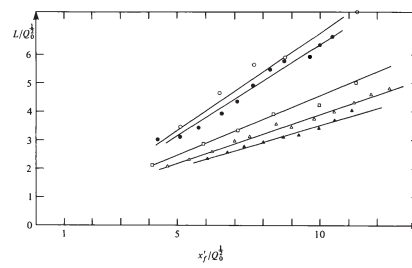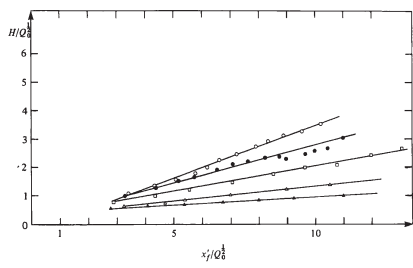

Figure 4: Dimensionless current height and length on slopes 5° (▲), 15° (△), 45° (), 60° (●), and 90° (○). From [1].
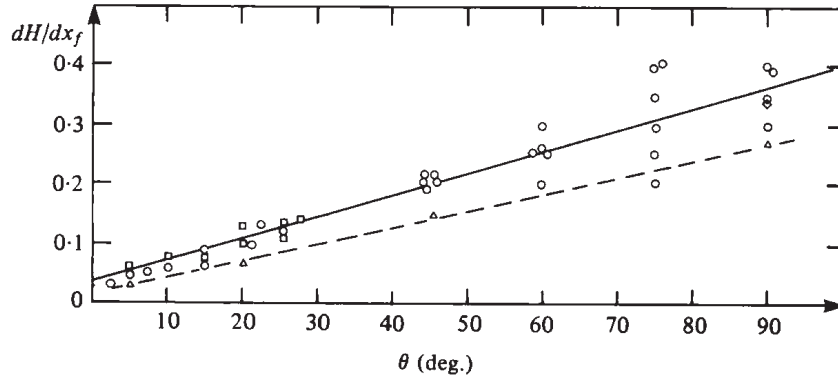
Figure 5: Increase in height as a function of slope. The dashed line is the current head measured by [3]. From [1].
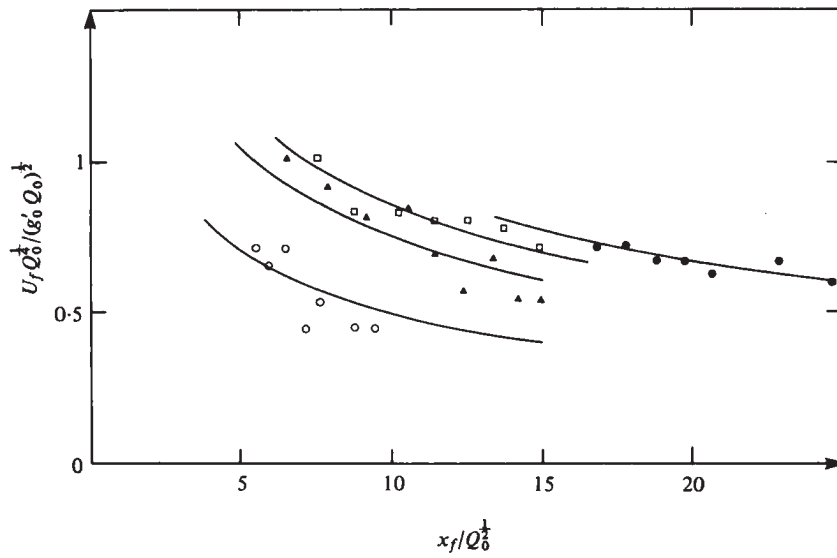

Figure 6: Dimensionless front velocity as a function of distance for slopes of 5° (•), 15° (),
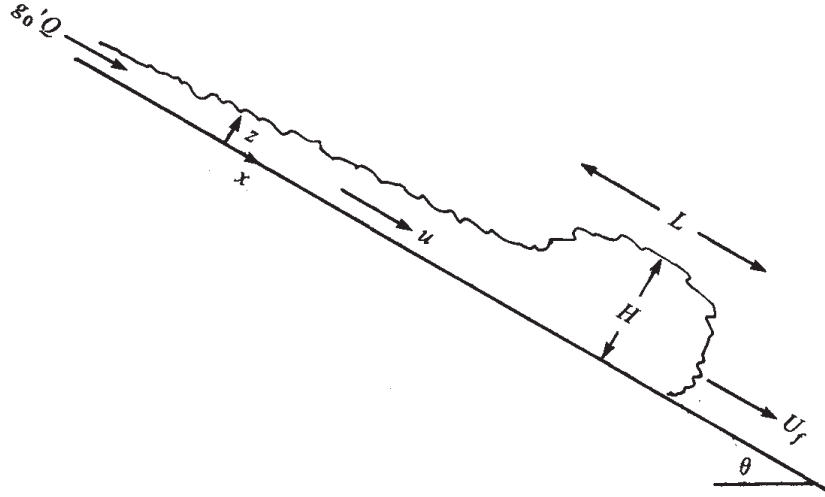45° (▲), and 60° (○). From [1].

5

Figure 7: Schematic of a constant flux gravity current down a slope. From [3].

2.2   Constant flux current

In a constant flux gravity current the rate at which volume is released down the slope is fixed. In this case the current usually exhibits a "head" at it's front, which can be characterized by dimensions L and H, followed by a long, thinner tail. A schematic of a constant flux current is shown in Figure 7 and images from an experiment are shown in Figure 8.

The relevant parameters in a constant flux current and their dimensions are

g'	reduced gravity (without taking slope angle into account)	$[L/T^2]$;
Q	volume flux / unit width	$[L^2/T]$;
θ	slope angle	no units.

Dimensionally then the velocity U of the current must be

$$U = \left(g'Q\right)^{1/3} f(\theta). \tag{3}$$

A plot the front position of a gravity current in time and a plot of U versus $(g'Q)^{1/3}$ showing the validity of this scaling are shown in Figure 9. A plot of the quantity $U/(g'Q)^{1/3}$ versus slope angle is shown in Figure 10 in an attempt to extract $f(\theta)$. While the data in Figure 10 is scattered, an examination of a similar plot for the speed of a cavity propagating in a fluid-filled tube, which perhaps represents the positive buoyancy case of a gravity current on a slope is shown in Figure 11, demonstrating well developed curves for $f(\theta)$. The growth rate of the height of the head at the front of the gravity current is plotted against slope angle in Figure 12. The entrainment rate as a function of slope and Richardson number is plotted in Figure 13. One interesting observation for the vertical current is that the entrainment and current shape is identical to a falling or rising plume which has been divided in half.

A persistent problem with the constant flux experiments is that it is difficult to obtain a high Reynolds number for the low angle flows in the lab such that the loss of momentum
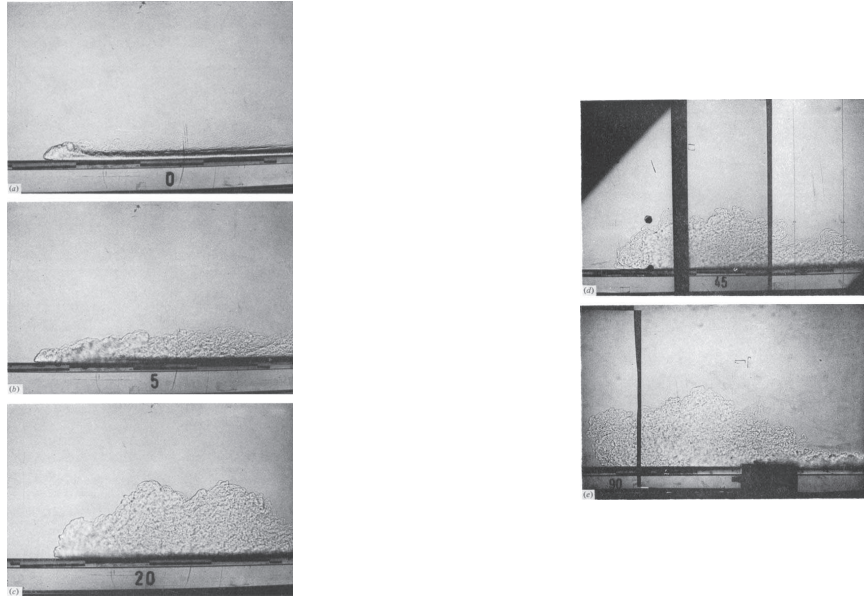
Figure 8: A constant flux gravity current flowing from right to left on slopes of 0, 5, 20, 45, and 90°. From [3].
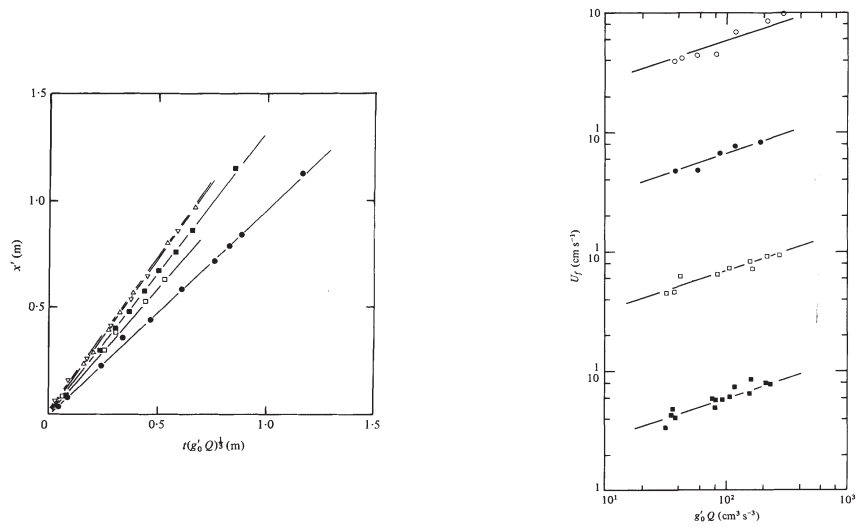

Figure 9: The front position of a gravity current on slopes of 0° (●), 5° (□), 20° (■), 45° (△), and 90° (▽). From [3].
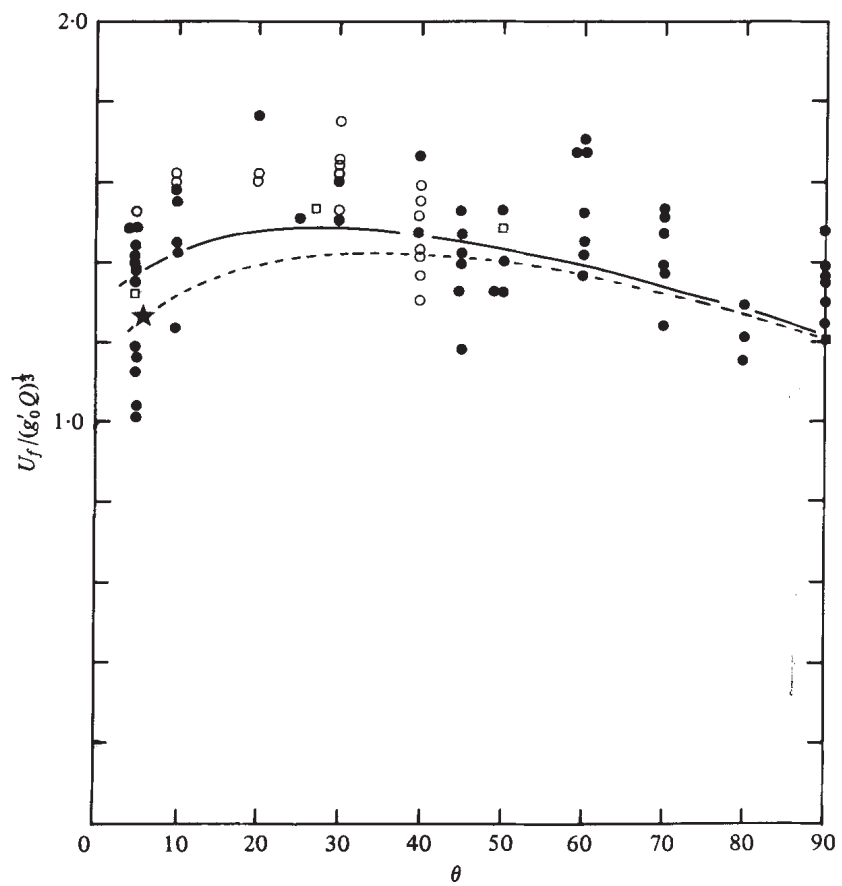
Figure 10: Non-dimensional front velocity $U/(g'Q)^{1/3}$ plotted against slope. $\star$ [5], [9], $\blacksquare$ [8], $\circ$ [7], $\bullet$ [3]. From [3].
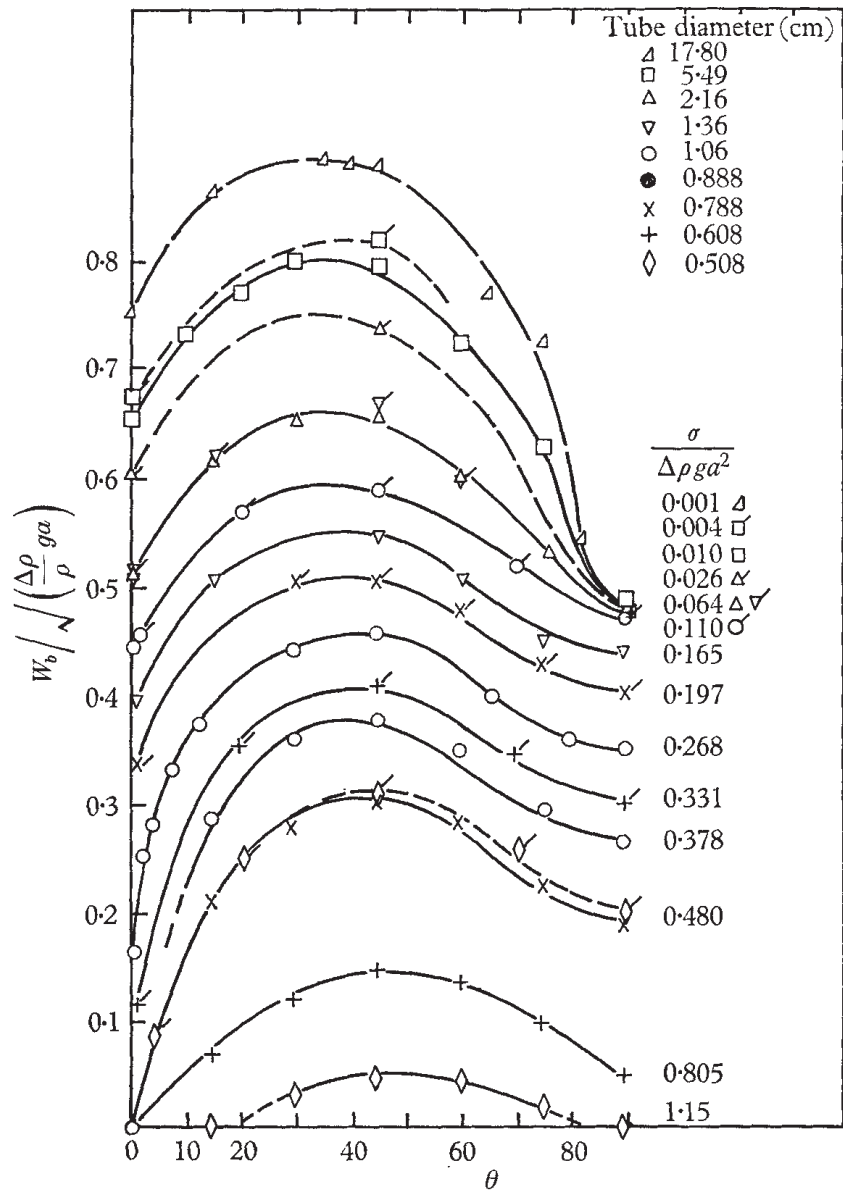
Figure 11: The speed of a cavity propagating along an emptying tube as a function of the angle of the tube axis to the horizontal. The speeds are expressed in terms of Froude numbers and the differences result from the effects of surface tension. In every case the maximum speed is at an inclination of 30° [10]
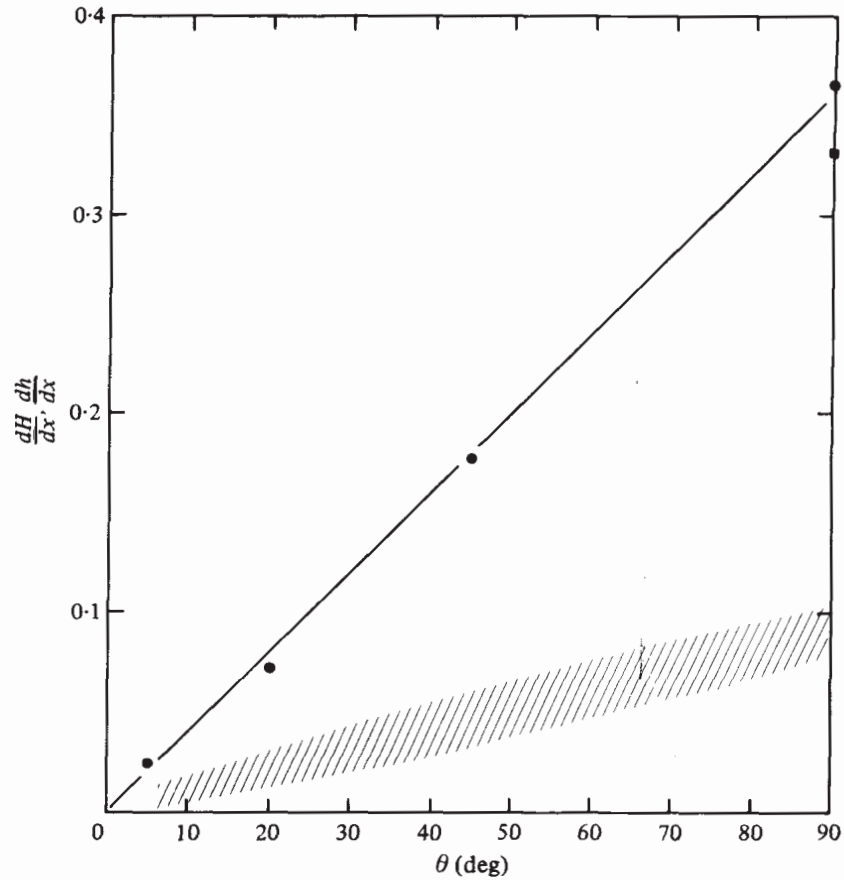
9

Figure 12: Growth rate of the head $\mathrm{d}H/\mathrm{d}x$ plotted against slope. The height of the following thinner layer is also shown by the shaded region (from [4]). From [3].
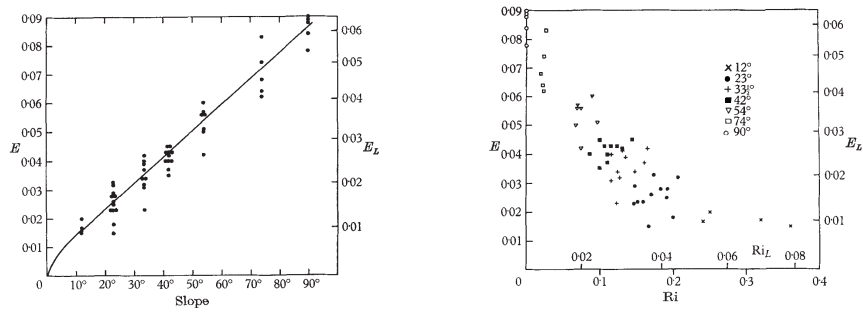

Figure 13: The entrainment rate measured in a continuous downslope flow as a function of slope angle and Richardson number Ri. From [4].
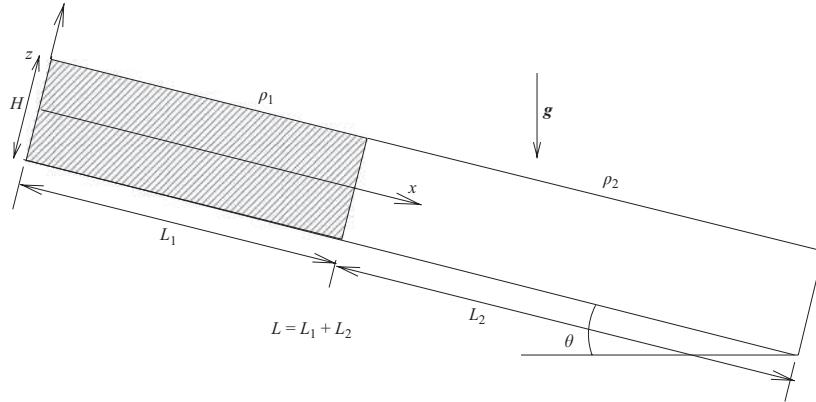
10

Figure 14: Lock exchange in a sloping channel [2].

due to bottom drag is not important. In many flows, additionally, we might expect a transition at some critical slope angle in the dominant factor controlling the velocity of the flow, from bottom drag to the loss of momentum due to the entrainment of ambient fluid. Additionally, because of the entrainment of ambient fluid, the velocity of the current is only a weak function of θ.

2.3   Lock exchange

We may also consider lock exchange in a sloping channel, which differs from the gravity currents considered above because of the addition of an upper boundary. A schematic of lock exchange in a sloping channel is shown in Figure 14. Similar to unconfined gravity currents on slopes, one of the most important differences induced by the slope is to make overturning and turbulent mixing more energetically favorable on the boundary between the two fluids. This is demonstrated by simulations (Figure 15) and experiments (Figure 16) and is especially evident at later times when the current becomes well-developed.
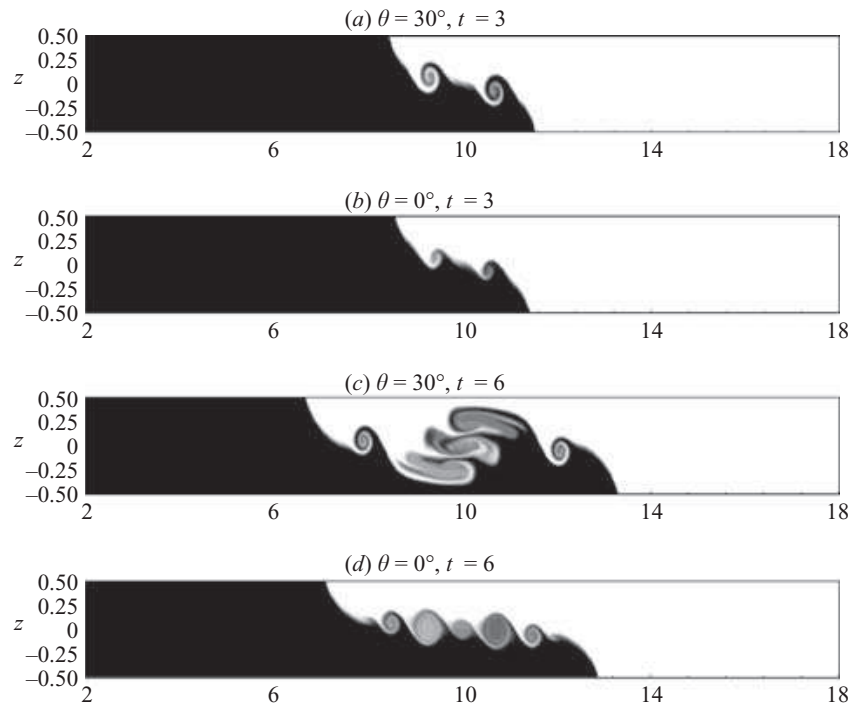
Figure 15: 2D DNS simulation of a Boussinesq sloping lock exchange for $\rho_1/\rho_2 = 0.98$ (where ρ_1 is on the right and ρ_2 is on the left) and $\Re = 4,000$ [2].
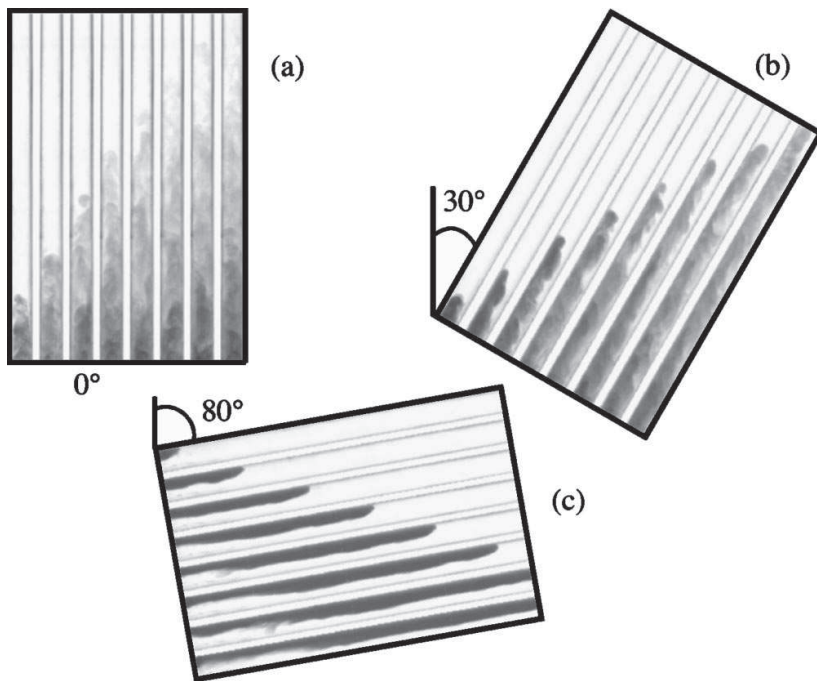
Figure 16: Images of sloping lock exchange at various angles for $\rho_1/\rho_2 = 0.992$. Note that $\theta = 90° - \alpha$, where θ is defined in the schematic in Figure 14 and α is the angle denoted in the images. From [6].

References

[1] P. Beghin, E. J. Hopfinger, and R. E. Britter, *Gravitational convection from instantaneous sources on inclined boundaries*, J. Fluid Mech., 107 (1981), pp. 407–422.

[2] V.K Birman, B.A. Battandier, E. Meiburg, and P.F. Linden, *Lock-exchange flows in sloping channels*, J. Fluid Mech., 577 (2007), pp. 53–77.

[3] R. E. Britter and P. F. Linden, *The motion of the front of a gravity current travelling down an incline*, J. Fluid Mech., 99 (1980), pp. 531–543.

[4] T. H. Ellison and J. S. Turner, *Turbulent entrainment in stratified flows*, J. Fluid Mech., 6 (1959), pp. 423–448.

[5] E. H. M. Georgeson, *The free streaming of gasses in sloping galleries*, Proc. Roy. Soc. A, 180 (1942), pp. 484–493.

[6] T. Séon, D. Hulin, J.-P.and Salin, B. Perrin, and E. J. Hinch, *Buoyant mixing of miscible fluids in tilted tubes*, Phys. Fluids, 16 (2004), pp. L103–L106.

[7] ——, *Buoyancy driven miscible front dynamics in tilted tubes*, Phys. Fluids, 17 (2005), pp. –31702.

[8] G. Tsang and I. R. Wood, *Motion of a two-dimensional starting plume*, J. Engng. Mech. Div. A.S.C.E., EM6 (1968), pp. 1547–1561.

[9] I. R. Wood, *Studies in unsteady self-preserving turbulent flows*, Tech. Report 81, University of New South Wales, Water Research Lab., 1965.

[10] E. E. Zukoski, *Influence of viscosity, surface tension and inclination angle on the motion of long bubbles in closed tubes*, J. Fluid Mech., 25 (1966), pp. 821–840.